Consequences of Striatal *Bmal1* Deletion on Dendritic Spine Morphology

Steven Dobric

A Thesis

in

The Department

of

Psychology

Presented in Partial Fulfillment of the Requirements

for the Degree of Master of Arts (Psychology) at

Concordia University

Montreal, Quebec, Canada

July 2022

CONCORDIA UNIVERSITY

School of Graduate Studies

This is to certify that the thesis prepared

By: Steven Dobric

Entitled: Consequences of Striatal *Bmal1* Deletion on Dendritic Spine Morphology

and submitted in partial fulfillment of the requirements for the degree of

Master of Arts (Psychology)

complies with the regulation of the University and meets the accepted standards with respect to originality and quality.

Signed by the final examining committee:

_____ Chair

C. Kristen Dunfield, PhD

_____ Examiner

Richard Courtemanche, PhD

_____ Examiner

Andrew Chapman, PhD

_____ Supervisor

Shimon Amir, PhD

Approved by:

_____

Chair of Department, Andrew Ryder, PhD

_____

Dean of Faculty, Pascale Sicotte, PhD

Date July 2022

ABSTRACT

Consequences of Striatal *Bmal1* Deletion on Dendritic Spine Morphology

Steven Dobric

Alterations to the circadian molecular clock that drive these rhythms are associated with the development of neurodegenerative diseases such as Alzheimer and Parkinson's disease and plays a key role in neuroplasticity (Cronin et al., 2017 & Perez-Cruz et al., 2009). Among the many genes involved in regulating circadian rhythms, *Bmal1* is vital for both the generation and maintenance of molecular circadian rhythms. Alterations to *Bmal1* functioning are associated with severe health concerns, such as motor impairments, metabolic syndrome, and a reduction in lifespan (Tonelli et al., 2009). The circadian system consists of a master pacemaker located in the Suprachiasmatic nucleus (SCN) of the hypothalamus, and peripheral clocks that synchronize to the master clock. Among these peripheral clocks is the striatum, a major site of synaptic plasticity, and a key player in motor control, and affective behaviors. Studies in our laboratory have confirmed that *Bmal1* is expressed in most neurons throughout the striatum (Frederick et al., 2017). Currently, our understanding of local circadian regulation on neuronal plasticity in the striatum is limited. By Golgi-staining striatal sections of *Bmal1* KO animals, we aim to understand the impact of deleting this crucial circadian gene on dendritic spine morphology. By utilizing the rotarod test, we also want to investigate the role of this gene in motor coordination. Results indicate that *Bmal1* deletion in the principal medium spiny neurons of the striatum has an impact on motor coordination and spine branching by reducing the density of spines and their junctions. However, no such differences were found between WT and HET animals, suggesting that *Bmal1* is haplo-sufficient in its role in striatal spine morphology. These results are the first to establish a role of *Bmal1* in striatal dendritic morphology and could have implications for future studies on striatal connectivity.

Acknowledgments

I am not even sure where I would like to start, there is so much to be thankful and grateful for. Shimmy, you have been incredibly supportive throughout my tenure in your lab. Time seems to have passed by so quickly, September will mark half a decade since you took me under your supervision. The trust you have put in me to develop this project from scratch, the time, and resources you invested in me, and the countless hours you spent reading over my work and meeting with me will never be forgotten. Your expertise in the field is unparalleled, and the feedback you offered me throughout this project has been invaluable. I am thankful for the opportunity you gave me to further my education, learn new and fascinating things, feeding my curiosity, and importantly for being a role model. I look forward to next year when I will be able to start my PhD and hope to continue working with you in the fruitful and competent way we have done so far. Finally, a big thank you to Nuria for her care, patience, and willingness to teach me whenever I needed teaching. I am saddened by your departure and wish you could have been here for the final steps of the project. I wish you nothing but the best in your future endeavors.

CONTRIBUTION OF AUTHORS

The experiments were designed by Steven Dobric and Dr. Shimon Amir. All experiments were conducted by Steven Dobric. Data was analyzed and interpreted by Steven Dobric with input from Dr. Shimon Amir. Data visualization was done by Steven Dobric. Manuscript was written by Steven Dobric, with editing by Dr. Shimon Amir.

Table of Contents

List of Figures

List of Tables

LIST OF ABBREVIATIONS

ANOVA: Analysis of variance

BMAL1*, *Bmal1: Brain and muscle arnt-like protein-1, or gene

cDNA: Complementary DNA

CK1 ε/δ: Casein kinase 1ε/δ

CLOCK, *Clock:* Circadian locomotor output cycles kaput protein, or gene

CNS: Central nervous system

CRE: cAMP/Ca2+ responsive element

CRY, *Cry:* Cryptochrome protein, or gene

CTR: Control

D1: Dopamine D1 receptor-bearing

D2: Dopamine D2 receptor-bearing

DA: Dopamine

EM: Electron microscopy

***Gpr88*:** G Protein-Coupled Receptor 88

HET: Heterozygote

KO: Knockout

MSN: Medium spiney neurons

PD: Parkinson's disease

PER, *Per:* Period protein or gene

RPM: Rotation per minute

SCN: Suprachiasmatic nucleus

SEM: Standard error of the mean

Tim: Timeless

TTFL: Transcriptional/translational feedback loop

WT: Wildtype

ZT: Zeitgeber (time giver)

The Impact of Striatal *Bmal1* Deletion on Dendritic Spine Morphology

Circadian rhythms are 24h oscillations in gene expression, physiology, and behavior that promote organismal fitness by enabling synchrony between the internal milieu and the physical and social environments. This synchrony between the organism's internal and external environments is critical to its survival (Vitaterna, et al., 2001). Circadian rhythms are generated endogenously by highly distributed networks of cellular circadian clocks and is a fundamental property of most living organisms. In mammals, critical physiological properties such as heart rate, blood pressure, hormone release, and sleep present temporal organization through the day (Garmabi et al., 2016). While other biological oscillations exist, these circadian oscillations are distinguishable because of the correspondence of their period with the 24h day cycle (Rusak & Zucker, 1979). Thus, the photoperiod is the most influential *Zeitgeber* (time giver) for the phase entrainment of circadian oscillators in organisms. The entrainment to solar time results from the innervation of the brain's central clock and photosensitive retinal ganglion cells that express the photopigment melanopsin (Berson et al., 2002).

The Master Pacemaker

The bilaterally paired suprachiasmatic nucleus (SCN) of the anterior hypothalamus is the primary circadian pacemaker of the mammalian brain and orchestrates various physiological processes. The SCN governs a distributed network of central and peripheral clocks and synchronizes their activity (Hastings et al., 2019). At the molecular level, the clock consists of an autonomous transcriptional/translational feedback loop (TTFL) involving a set of clock genes which are regulated by their own protein products (Takahashi, 2017). Heterodimers of the transcription factors BMAL1 and CLOCK form the positive arm of the loop and drive the expression of *Period* (PER) and *Cryptochrome* (CRY) through specific binding to E-boxes in the

promoter region of these genes (Reppert & Weaver, 2001). Upon transcription in the nucleus and subsequent translation in the cytoplasm, PER and CRY proteins form a complex that re-enters the nucleus and inhibits the actions of BMAL1/CLOCK thereby forming the negative arm of the feedback loop. Kinases such as casein kinase 1ε/δ (CK1 ε/δ) regulate the activity of PER-CRY dimers at a post-translational level. In the absence of any external or environmental input, this autoregulatory feedback loop cycles every 24h (Albrecht, 2012).

Peripheral Synchrony

The SCN clock synchronizes peripheral clocks found in nearly every cell of the central nervous system (CNS) and organ system throughout the body. Brain regions outside the SCN with rhythmic expression of clock genes include the thalamus, hypothalamus, olfactory bulbs, cerebellum, and striatum. Complex autonomous oscillatory networks found in peripheral organs drive key physiological rhythmic processes such as detoxification by the kidneys and metabolism in the liver (Dibner et al., 2010). This interplay between the master pacemaker and peripheral clocks is necessary in maintaining robust circadian rhythms and promoting cellular homeostasis (Barclay, Tsang & Oster, 2012). Misalignment between the SCN and peripheral clocks has been associated with the etiology of metabolic syndrome and neurodegenerative disorders (Chauhan et al., 2017).

The Striatum

The striatum is a major site of synaptic plasticity and has a key role in motor control and affective behaviors. *Bmal1*, the only indispensable clock gene in mammals, is expressed in medium spiney neurons (MSNs), a type of GABAergic inhibitory neurons that represent ~95% of cells in the striatum (Frederick et al., 2017). Recent findings from our laboratory have found that striatal *Bmal1* influences alcohol consumption in a sexually dimorphic manner (de Zavalia et

al., 2021). Altered circadian rhythms and disruption in striatal clock gene expression also contributes to the symptomology of striatum-related mood disorders (Kim et al., 2017). The rhythmicity of clock gene expression in the striatum is sensitive to dopamine (DA) changes which has potential implications for mood disorders (Hood et al., 2010). Despite the expression of clock genes in the striatum, very little is known about their functions.

The Circadian System in Neuroplasticity

Beyond its role in circadian physiology, the circadian system also functions as a key element in cytoarchitectural organization and neuroplasticity. Research has also found that the circadian clock modulates dendritic structural plasticity in the lamina of *Drosophila melanogaster.* Specifically, dendrites appear to be longer and form a more complex network in the daytime. However, this rhythmicity is not present in arrhythmic per^{01} mutants (Weber et al., 2009). Research has also found that the basilar dendrites in the rat infralimbic cortex were longer and more complex during the active (dark) period than during the animal's rest period (light) (Perez-Cruz et al., 2009). Similarly, a study by Tovar and colleagues (2018) showed through temporal analysis of hippocampal dendritic structure in Siberian hamsters that photoperiod dependent morphological changes occur during the active phase in CA1 hippocampal pyramidal neurons. Specifically, shorter days (8h light:16h dark) cause a significant increase in dendritic branching complexity than longer days (16h light:8h dark). Synaptic plasticity also appears to be under circadian control, where the size of hippocampal synaptic dendritic spines increases during the dark phase in rodents (Tovar et al., 2018). However, while these links between clock genes and neuroplasticity have been made, it is difficult to distinguish if these changes are due to a direct or indirect effects of clock genes, namely through the many downstream effects of clock

genes. Nevertheless, it appears that the circadian system plays an integral role in cytoarchitectural organization and dendritic plasticity.

Despite the rhythmic expression of clock genes being found throughout the CNS, little is understood about their function outside of the SCN. Particularly, while the circadian system as a whole plays an important role in cytoarchitectural organization, it is unknown what function circadian genes have in striatal dendritic spine plasticity. Here, we provide evidence that disruption to the striatal molecular clock causes aberrated dendritic spine morphology. This was achieved by examining the density, number of junctions, and average length of dendritic spines following the conditional knockout of *Bmal1* in MSNs using the Cre-Lox recombinase system. Our results demonstrate that the striatal molecular clock is important in maintaining striatal dendritic morophology. These findings could have implications for mental and neurodegenerative disorders associated with changes in spine density and cortical connectivity (Garey et al., 1998).

Methods

Animals

Conditional *Bmal1* knockout mice were generated in our laboratory using the Cre-lox recombination system as described before (de Zavalia et al.,2021). In brief, *Gpr88*(Cre/+) male mice were bred with *Bmal1* floxed (fl/fl) female mice to generate heterozygote F1 offspring (*Gpr88*Cre/+; *Bmal1*fl/+). Next, F1 males were crossed with *Bmal1*(fl/ fl) females to produce experimental and control animals. Conditional *Bmal1* knockout mice (*n*=4) (*Gpr88*Cre/+; *Bmal1*fl/fl [*Bmal1*KO]), heterozygote (*n*=4) (*Gpr88*Cre/+; *Bmal1*fl/+ [*Bmal1*HET]), and wild type control animals (*n*=4) (*Gpr88*+/+; *Bmal1*fl/fl [*Bmal1*CTR]) male mice were used for experiments with an age of 12–18 weeks. Note, *Gpr88* is an orphan G-protein couple receptor

that is almost exclusively expressed in striatal MSNs. Thus, conditional knockout is restricted to this population of neurons (de Zavalia et al., 2021). However, because of recombination events at the *Bmal1* locus caused by Cre during germ cell development, control and experimental animals only had one functional copy of *Bmal1* genome-wide (Schöttner et al., 2022). Genome-wide genotypes were as followed: *Bmal1* conditional KO, (*Gpr88*cre/+; *Bmal1*-/fl) and *Bmal1* controls (CTRL, *Gpr88*+/+; *Bmal1*-/fl). In order to rule out that motor and physiological alterations in *Bmal1* KO animals were a result of *Gpr88* haploinsufficiency, *Gpr88*Cre/+ (*n*=3) and corresponding controls (Grp88+/+) (*n*=4) were assessed as well.

Mice were group-housed (2–4 individuals) under a 12:12 h light-dark cycle (08:00 am to 08:00 pm) and had access to water and standard rodent chow ad libitum. All animal experiments and procedures were conducted in accordance with the guidelines set by the Canadian Council of Animal Care and by the Animal Research Ethics Committee of Concordia University.

Gene Expression Confirmation

As previously described, knockout confirmation and validation of our *Bmal1* KO line was conducted in our laboratory. Immunofluorescence microscopy was performed on 30 µm, formaldehyde-fixed coronal sections. Sections were stained using antibodies against *BMAL1* and Alexa-conjugated secondary antibodies and visualized in an Olympus FluoView FV10i confocal microscope (Figure 1) (de Zavalia et al., 2021)

For gene expression, brains were harvested, and tissue punches of the dorsal striatum were isolated and subjected to RNA extraction and cDNA synthesis followed by quantitative PCR. qPCR was performed using primers against exon 8 of *mBmal1.* Amplification detection was performed using an Illumina Eco as previously described (Figure 3).

Motor Coordination Assessment

To assess motor coordination, animals underwent a habituation trial and three experimental trials on the rotarod test. In total, 4 control, heterozygote, and knockout animals underwent the experiments. Each animal was placed on a rotating rotarod covered with chloroethylene to prevent them from gripping onto it. Each animal underwent a habituation trial on the rotarod rotating at 1 rotation per minute (RPM). Upon successfully completing the habituation trial, animals underwent the experimental trials. Animals had one attempt to stay on the rotarod for as long as possible at varying RPMs. Upon successfully staying on the rotating rod for 180s, animals were taken off. If an animal failed to stay on the rod, latency to fall off and total time spent on rotarod were marked. Each animal began the first step at 2 RPM, followed by 4 RPM, 8 RPM, and 12 RPM. Upon completing the 12 RPM step, animals were given a 20-minute break and the next trial began. This was repeated three times for each animal, and total time spent on rotarod and latency to fall off were recorded.

Golgi Staining and Slicing

The Golgi-Cox method was used to study and quantify various dendritic morphological properties. This method confers several advantages compared to fluorescent- based neuronal labeling. Golgi staining can be applied to any tissue, is readily and easily available to researchers with a simple light microscope and camera, can be acquired more rapidly, and Golgi-stained samples are viable for extended periods of time (Risher et al., 2014).

The protocol used was as described by Zagout and Kaindl (2016). In brief, all impregnation solutions were prepared before each experimental day. Mice were decapitated at ZT 13 (9pm) and brains were carefully removed and washed in double distilled H_20. The cerebellum and olfactory bulbs were cut using a brain matrix and brains were transferred into individual 15ml falcon tubes containing equal parts of the impregnation solutions A and B. After

24h, brains were transferred into new 15ml falcon tubes containing solutions A/B. Brains were kept in the dark for two weeks before being transferred into solution C. Again after 24h, brains were transferred into new 15ml falcon tubes containing solution C and kept in the dark for 4 days.

Brain sections were cut using a cryostat. Brains were removed from solution C and flash frozen using -70ºC isopentane. Frozen tissues were mounted on disc specimens using tissue mounting medium and kept on dry ice for 15 minutes to prevent them from thawing. 200-µm sections of the dorsal striatum were cut according to the mouse atlas (Interaural ~3.94mm, Bregma ~0.14mm). Sections were immediately mounted on gelatin-coated microscope slides and kept in the dark for 24h to allow sections to dry.

Sections were rinsed twice for 4 minutes in double distilled water then immersed for 10 minutes in equal parts of staining solutions D and E. Sections were rinsed again twice for 4 minutes in double distilled water and dehydrated once in each following ethanol concentration for 4 minutes: 50%, 75%, 95%, and 99%. Sections were then cleared in xylenes 3 times for 4 minutes. Finally, sections were mounted on gel-coted glass slides and cover-slipped using Permount.

Imaging and Morphological Analysis

Images of dorsal striatal sections (Interaural ~3.94mm, Bregma ~0.14mm) of each animal were captured using a Nikon Ti inverted microscope with brightfield trans-illumination, a 60X PlanApo lambda objective lens (NA1.45) with 1.5x zoom relay lens. Focus-stacked images were captured with a Nikon DSRi2 camera in 3x3 binning mode (0.1µm/pixel), with 0.3µm Z-spacing. Sections imaged were randomly selected based on three criteria established by Risher and colleagues (2014). Ideal dendritic section were at least 10 microns in length, uninterrupted,

and dendritic spines were all visually distinct from one another. In total, 10 randomly selected dorsal striatal sections were captured for each animal.

Dendritic segments identification and measurements were all done in FIJI using the skeletonization plugin. First, ND2 Nikon TiE image files were exported into FIJI and Z-stack images were compressed into single binary-colored images. Clear dendritic segments were identified and subsequently selected using the "rotated rectangle" tool. Segments lengths were measured using the "freehand selection" tool, and lengths in microns were noted. Next, pixel intensity threshold was adjusted using the "threshold" function to delineate between background noise and foreground information. Images were then skeletonized using the "perform skeletonization" function, and the dendritic segments were then analyzed using the "analyze skeleton" function. This function measures four important characteristics; number of junctions, average spine length, and average shortest/longest spine. Note, a junction was counted in the analysis when a voxel had at least 2 neighboring voxels. Raw data was imported directly into an excel spreadsheet. Finally, spine density was calculated by taking the total spine count and dividing it by the length of the dendritic segment (Figure 4).

Data Analysis

All data analysis was performed in IBM SPSS v28. Results were depicted as mean ± standard error of the mean (SEM). Motor coordination tests were analyzed using a repeated measure analysis of variance (RM-ANOVA) followed by Tukey's multiple comparison. All morphological parameters in WT, HET, and KO animals were analyzed using two-way ANOVAS (parameter and genotype effect) followed by Tukey's multiple comparisons. Morphological parameters in the *Gpr88* +/+ and *Gpr88*Cre/+ validation animals were analyzed

using a one-way ANOVA. All relevant assumptions were assessed and discussed in the results section.

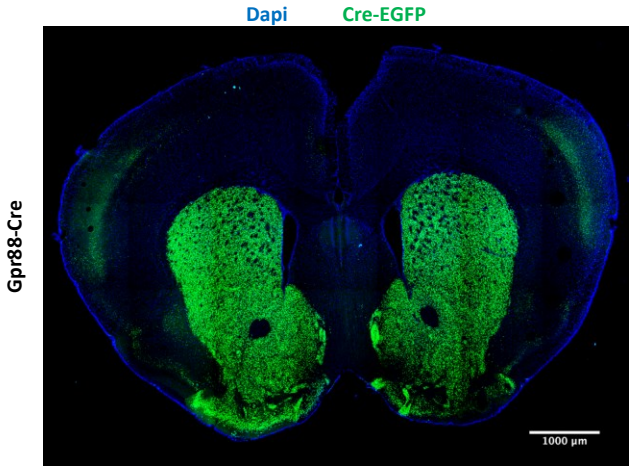

*Figure 1. Cre-EGFP expression in a Gpr88-Cre mouse***.** Cre expression (green) is localized to the dorsal striatum, nucleus Accumbens, and olfactory tubercle.

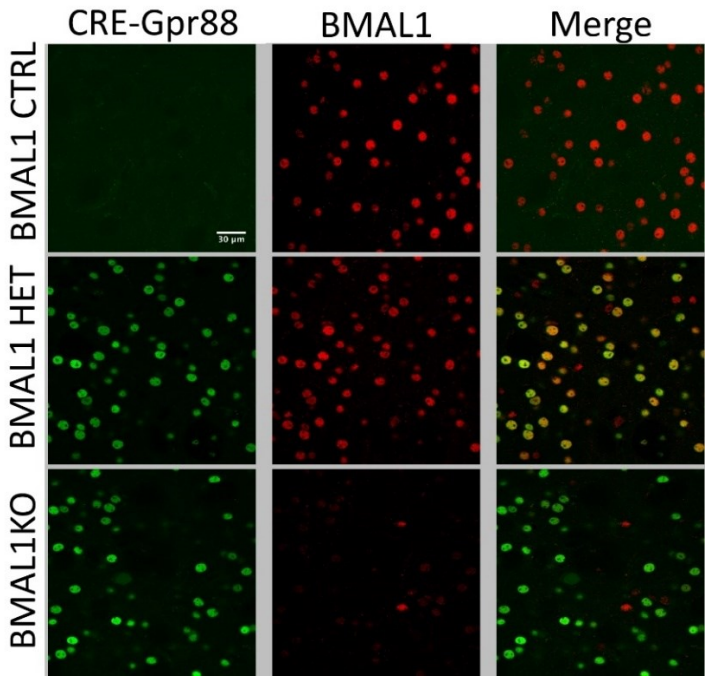

Figure 2. Cre-EGFP and Bmal1 expression. Representative image of BMAL1 immunofluorescence staining in dorsal striatal tissue of control, *Bmal1* heterozygote, and knockout mice. BMAL1: red, *Gpr88*-Cre-GFP: green. (de Zavalia et al., 2021).

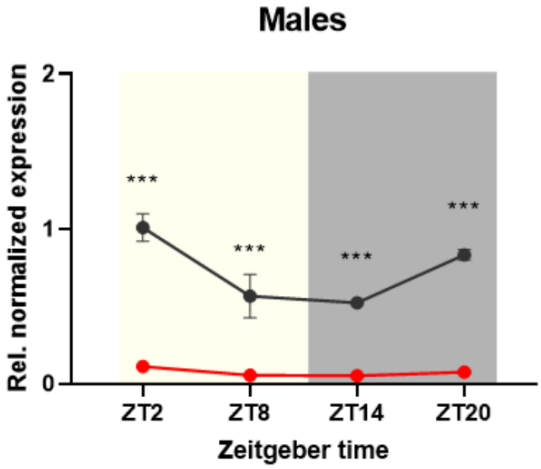

Figure 3. qPCR validation of Cre-mediated excision of Bmal1 from the dorsal striatum. Data shows *Bmal1* mRNA expression across the day in control (black line) and KO (red line) animals. Zeitgeber time 2 represents the time two hours after light onset. 3-4 animals per genotype and timepoint. *** indicates significance at $p<0.001$. $F(1,36) = 366.6$, $p < 0.0005$ (Schöttner et al., 2022).

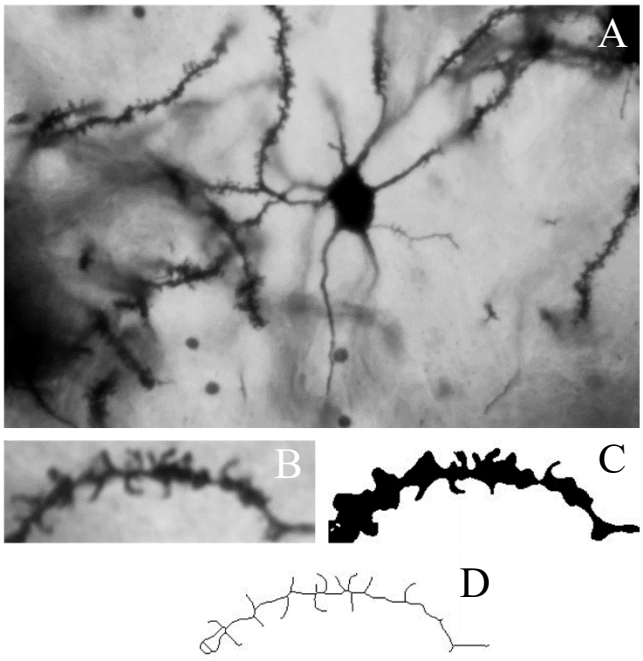

Figure 4. Stepwise process of capturing and processing striatal dendritic segments. **A.** Clear and randomly selected neurons from the dorsal striatum were captured using 40x magnification. **B.** One dendritic segment per neuron was selected based on the criteria established by Risher and colleagues (2014). 10 segments from different neurons were captured for each animal using 90x magnification (60X lambda objective lens with 1.5x zoom relay lens). **C.** Segments were processed and analyzed in FIJI. Color thresholds were adjusted to delineate between background noise and foreground information. **D.** Skeletonization of threshold-adjusted segments allowed for spine density, number of junctions, average spine length, and average shortest/longest spine length quantification.

Results

Data Integrity

All statistical analyses were performed in IBM SPSS v28. All missing data points were coded as -999 and excluded from analysis. Data were checked for severe outliers, two were identified in the "average density" and "number of junctions" variables and were subsequently removed (±3 standardized z scores) (Kline, 2009). All other relevant assumptions for each test were verified and reported in their corresponding sections.

Motor Coordination

(±3 standardized z scores) (Kline, 2009. Each animal was weighed before the rotarod test and a one-way ANOVA demonstrated no statistically significance differences between genotypes, $F(2,9) = 0.574$, $p = .583$ (Figure 5).

A 3 x 4 mixed repeated-measures ANOVA was performed to assess the influence of the between-subjects variable "genotype" (WT, HET, KO) and the within-subjects variable "time taken to fall from the rotarod" at varying speeds (2RPM, 4RPM, 8RPM, 12RPM). A one-way ANOVA followed by a Tukey post-hoc test for multiple comparison was used to assess differences in total time spent on rotarod across genotypes.

Relevant assumptions for a one-way ANOVA include homogeneity of variance and independent observations. The latter is not relevant in our study due to the homogeneous nature of our animal sample. Normality is also a non-issue, as ANOVAs are generally robust to non-normality and any transformations to render the sample normal will result in a loss in the meaningfulness of the metric (Kline, 2009). Finally, Levene's test indicated a homogenous variance, $F(2,8) = 2.452$, $p = .148$. There was a significant effect of genotype on total time spent on rotarod, $F(2,8) = 4.607$, $p = .047$, $\eta 2 = .535$. A Tukey post hoc for multiple comparison

revealed that the total time spent on rotarod was significantly higher in HET than KO mice (p = [0.041], 95% C.I. = [10.448; 449.551]. There were no statistically significant differences between WT and KO mice (Figure 5) (appendix A).

Relevant assumption for a repeated measure ANOVA includes sphericity and independent observations. Mauchly's test indicated that the assumption of sphericity had been violated χ^2 (5) = 12.719 p =.028, and thus Greehouse-Geisser values are reported. There was a statically significant main effect of rotarod speed on latency to fall, F (2.038, 16.306) = 11.812, p < .001, partial η2 = .596, where animals performed worst as the RPM increased. However, there were no statistically significant differences in the interaction between RPM*Genotype, F (4.077, 16.306) = .717, p = .595, partial η2 = .152 (appendix A) (Figure 5). The failure to find significance is likely due to the small sample size and large variance.

Dendritic Morphology

Dendritic parameters examined include dendritic spine density, number of spine junctions, average spine length, and average shortest/longest spine length as established by Smith et al., (2009). All measurements were performed in FIJI vJava8 using the skeletonization extension. Raw data files were exported and cleaned in Excel. All analyses were performed in SPSS v28. Total imaging sample size was n = 190, where 10 images were captured for each animal.

A one-way ANOVA followed by a Tukey post-hoc tests for multiple comparison were used to assess differences in dendritic morphology. Levene's test indicated a homogeneous variance across all parameters (appendix B). First, there was a statistically significant effect of genotype on average spine density F(2, 114) = 11.554, p = <0.001, η2 = .169. Specifically, KO animals had a significantly lower density of spines than WT animals (p = [<0.001], 95% C.I. =

[0.054; 0.16]. There were no differences between HET and WT animals (p = [.094], 95% C.I. = [-.006; .099]. There was also a statistically significant effect of genotype on number of junctions $F(2, 114) = 9.203$, $p = <0.001$, $\eta 2 = .139$. Specifically, WT animals had significantly more junctions than KO animals (p = [<.001], 95% C.I. = [2.33; 8.33]. There were no differences between WT and HET animals (p = [.341], 95% C.I. = [-1.22; 4.75] (Figure 6, appendix B). Finally, there was no effect of genotype on average length of dendritic spines, including for both average shortest and average longest spine (Figure 7, appendix B).

As mentioned, to rule out the possibility that morphological differences in *Bmal1* KO animals were a result of striatal *Gpr88* haploinsufficiency, *Gpr88*Cre/+ and corresponding controls (*Grp88*+/+) were assessed. As previously described, no motor deficits were found in our *Gpr88* lines (Schöttner et al., 2022). A one-way ANOVA was used to assess morphological properties across both genotypes. Levene's test indicated a homogeneous variance across all parameters. We found no effect of genotype on any of the morphological parameters (Figure 8 & 9). Thus, we can rule out the possibility that morphological differences in *Bmal1* KO animals were a result of *Gpr88* haploinsufficiency (appendix C).

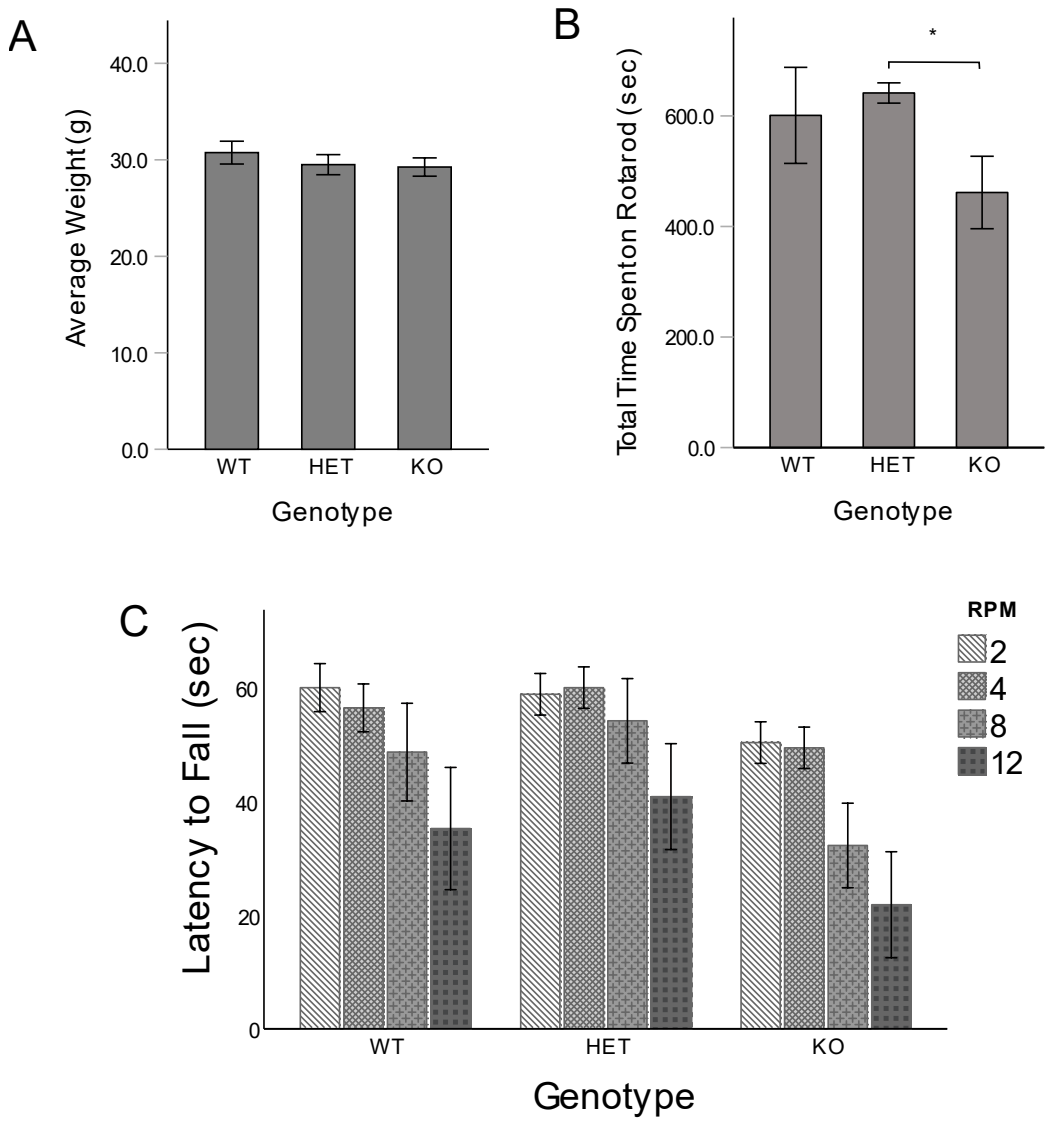

Figure 5. *Body weight, total time spent on rotarod, and time taken to fall off across different speeds between genotypes*. **A.** There was no difference in weights across genotypes. **B.** There was a statistically significant effect of genotype on total time spent on rotarod between HET (n = 4) and KO (n = 4) $p = 0.041$. **C.** There was a statically significant main effect of rotarod speed on latency to fall, p=<.001, however there were no statistically significant differences in the interaction between RPM*Genotype. Error bars represent SEM. p<.05 *

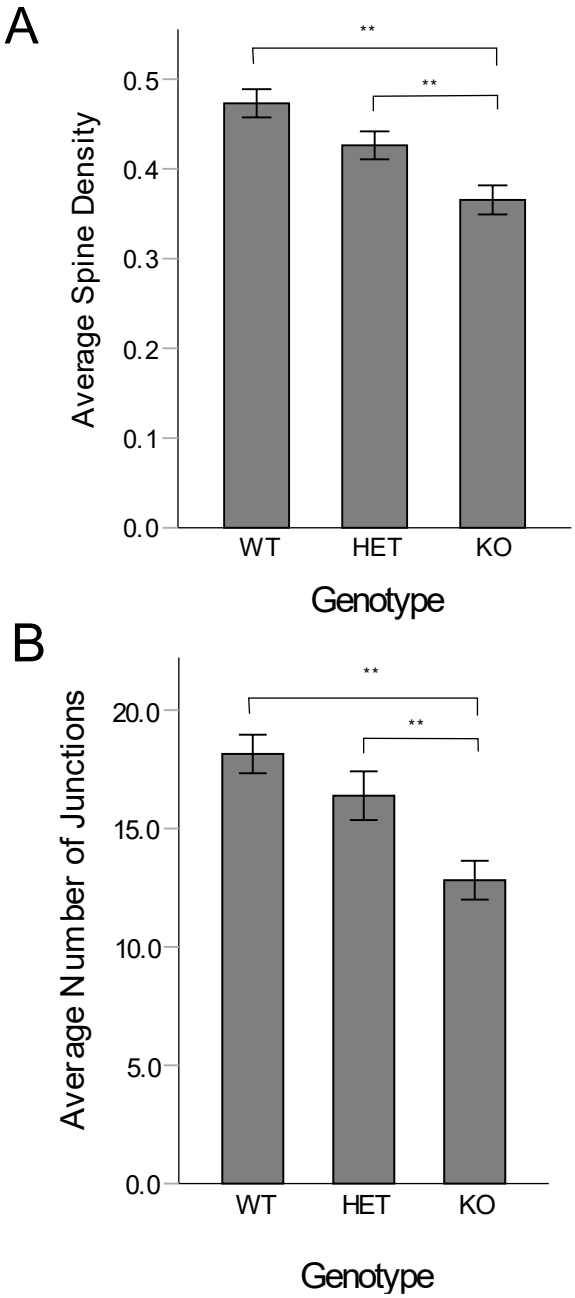

Figure 6. *Spine density and number of junctions across genotypes*. **A.** There was a statistically significant effect of genotype on spine density between WT and KO animals, p=<0.001. **B.** Similarly, WT animals also had a statistically significant greater number of junctions than KO animals, p=<0.001. Error bars represent SEM. p<.001 **

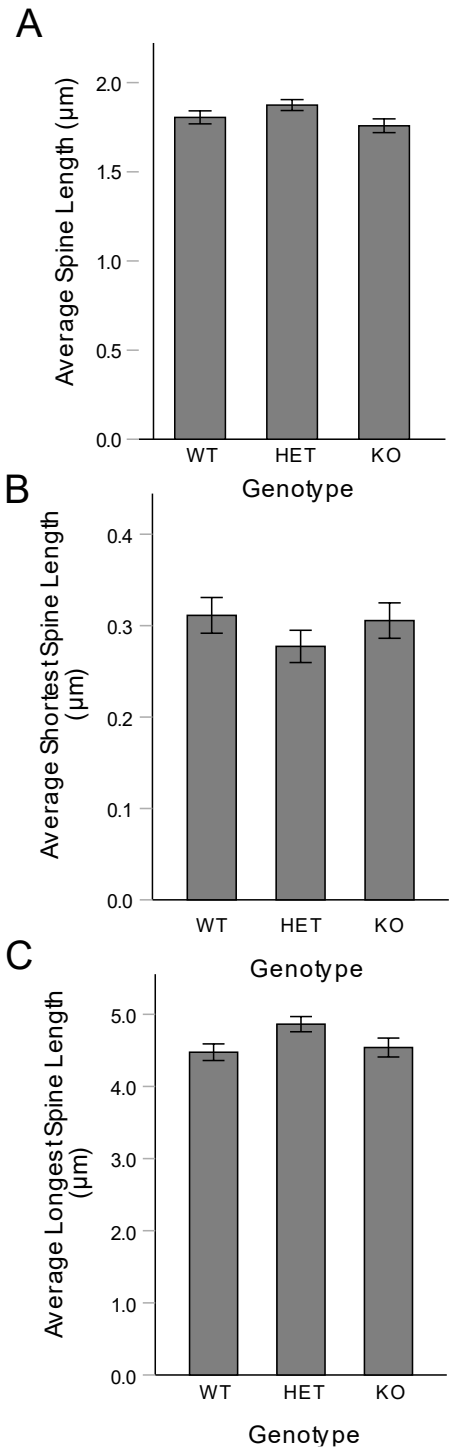

Figure 7. *Dendritic spine lengths across genotypes*. There were no statistically significant differences in average, shortest, or longest spine length across genotypes. Error bars represent SEM.

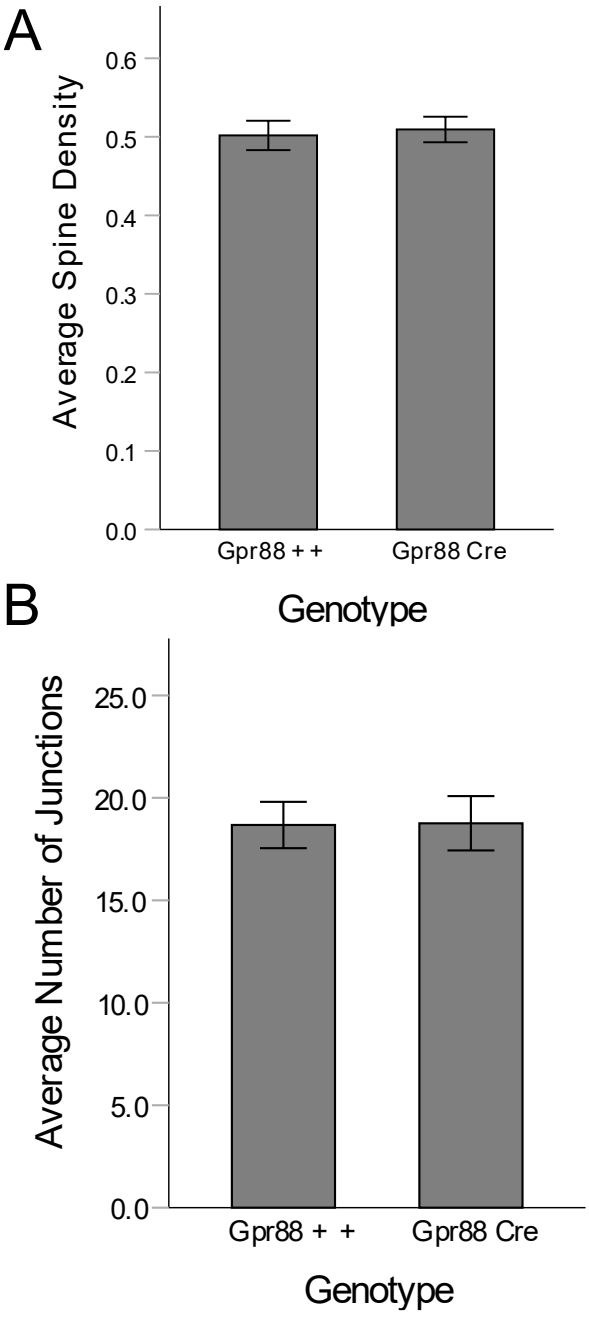

Figure 8. *Spine density and number of junctions in Gpr88 + + and Grp88 Cre animals*. There were no statistically significant differences in spine density or number of junctions. Error bars represent SEM.

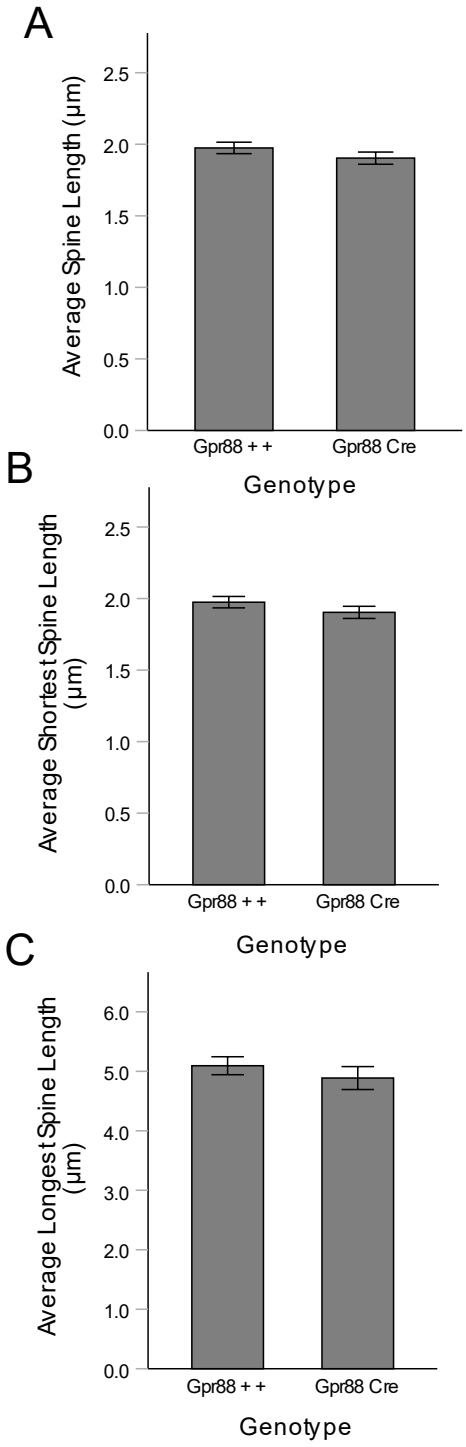

Figure 9. Dendritic spine lengths between Gpr88 +/+ and Gpr88 Cre animals. There were no statistically significant differences in average, shortest, or longest spine length across genotypes. Error bars represent SEM.

Discussion

The impact of a conditional knockout of *Bmal1* from MSNs, the principal neuron of the striatum, on locomotor activity and dendritic spine morphology was assessed in the present study. Results were validated in *Gpr88* mice to rule out the possibility that motor and spine phenotypes observed in *Bmal1* KO mice were the effect of *Gpr88* haploinsufficiency. *Grp88(cre/+)* mice lack one functional copy of the *Gpr88* gene but have complete clock gene expression, whereas *Grp88(+/+)* mice have both *Gpr88* genes intact and complete clock gene expression. Previous findings in Drosophila by Weber et al., (2009) and Perez-Cruz et al., (2009), have shown that the density, length, and overall complexity of dendritic spines express circadian rhythmicity governed by clock genes. Specifically, Per^{01} mutations, an important circadian gene, have been associated with aberrated dendritic spines. Circadian plasticity also extends to rodents, where the density of dendritic spines in pyramidal CA1 neurons vary rhythmically (Ikeda et al., 2015). Robust circadian plasticity has also been observed in the somatosensory cortex of mice, where the density of excitatory synapses and their spines are greater during the active period (dark) than the rest period (light) (Jasinska et al., 2014, 2015). Given the importance of clock genes in the rhythmic change of cortical plasticity, and extensive evidence of the role of striatal circuitry in motor functioning, we hypothesized that dysregulation of striatal clock gene expression would result in aberrated motor coordination and dendritic spine morphology.

Motor function

Deficits in motor coordination in the rotarod test following *Bmal1* KO were previously reported in our laboratory (Schoettner et al., 2022). Similarly, we found an effect of genotype, where *Bmal1* KO mice spent less time on the rotarod than HET animals. However, no such

effects were observed between WT and KO animals, likely due to the small sample size and high variance. Finally, there was no genotype X RPM interaction. Again, this is likely due to a small sample size and high variance. We expect that increasing the sample size would result in a significant interaction, particularly in differences between WT and KO and HET and KO.

While previous studies reported an effect of *Gpr88* knockout on motor functioning (Quintana et al., 2012; Meirsman et al., 2016a, 2019), no differences were found between our *Gpr88+/+* and *Gpr88cre/+* animals. These results confirm that the observed disruption in motor functioning in this study were caused by loss of function in *Bmal1* and not by *Gpr88* haploinsufficiency.

Severe motor abnormalities are linked with striatal neurodegenerative disorders such as Parkinson's Disease. However, animal models of PD often involve lesioning of the nigrostriatal dopaminergic pathway, making it difficult to conclude causal effects between motor deficiencies and the animal model given the extent of the damage (Alonso, 2021). Given that our model does not lesion the nigrostriatal dopamine pathway, we can more soundly conclude that disruption in striatal functioning due to loss of function of *Bmal1* causes impairments in motor coordination.

Dendritic Spines

Dendritic parameters examined included spine density, number of spine junctions, average spine length, and average shortest/longest spine length, as established by Smith et al., (2009). The present study provides novel findings on the impact of striatal *Bmal1* deletion on the aforementioned parameters. Specifically, although the length of the spines remains unaffected by *Bmal1* deletion, *Bmal1* has a role in dendritic spine density and number of spine junctions, as suggested by the finding that conditional *Bmal1* KO results in aberrated spine branching.

Dendritic spine density and average number of spine junctions were both negatively impacted by the deletion of *Bmal1*. Interestingly, comparing both WT and HET with KO animals, we saw a significant reduction in branching. However, there were no differences between WT and HET animals. This shows that *Bmal1* is haplo-sufficient regarding its role in spine branching, a finding that could have important implications in striatal neurodegenerative disorders such as in PD where cytoarchitectural phenotypes are marked by dendritic degeneration. Milatovic et al., (2005) reported that both dendritic length and dendritic spine density were significantly reduced in striatal medium spiny neurons of PD patients. To our knowledge, the present study is the first to demonstrate the impact of striatal *Bmal1* deletion on dendritic spine morphology. These results have potential implications for understanding the relation between *Bmal1* expression in the striatum and late-stage structural changes in MSNs of PD patients.

We did not find any differences in the average length of spines, including both average shortest spines and average longest spines. These findings are at odds with a previous study in Drosophila, which reported that disruption in clock gene expression was associated with a reduction in dendritic length (Weber et al., 2009). There are three possible explanations for our findings. First, the authors investigated only the length of the dendritic segment and not the spines. It is possible that different mechanisms mediate the branching properties of dendrites and spines. Second, the authors conducted their study in Drosophila whereas our experiments were carried out in mice, and there could be species differences in mechanisms that link clock genes with dendritic plasticity. Third, we only examined the deletion of *Bmal1*, one of several circadian genes reported to have a role in neuroplasticity (Krzeptowski et al., 2018). One hypothesis is that

different circadian genes control different properties in striatal MSN morphology. Future studies need to examine the effect of other circadian genes on striatal dendritic spine morphology.

Gene expression and *Gpr88* animals

Our *Bmal1* KO mice have only one functional copy of *Gpr88*; the other copy has been altered to express Cre. Previous studies have reported various deficits associated with the global knockout of *Gpr88*. Namely, a deficit in motor functioning, increased alcohol seeking behavior, and poor anticipatory behavior (Quintana et al., 2012, Hamida et al., 2018, Maroteaux et al., 2018). To rule out the possibility that any motor and/or morphological alterations in *Bmal1* KO animals were a result of *Gpr88* haploinsufficiency and associated changes in behavior, *Gpr88*Cre/+ (n=3) and corresponding controls (*Grp88*+/+) (n=4) were assessed. We found that in contrast to *Bmal1* KO animals, the loss of one copy of *Gpr88* did not affect any of the morphological parameters examined. As reported by Schoettner et al., (2022), no motor deficits in the rotarod were found either in the *Gpr88* mice. Given this, we can conclude that the resulting phenotypes observed in KO animals is due to a lack of striatal *Bmal1* expression rather than *Gpr88* heterozygosity.

Limitations and future directions

MSNs of the striatum can be divided into two main subtypes, dopamine D1 receptor-bearing (D1) and dopamine D2 receptor-bearing (D2). Research has demonstrated that D1 and D2 receptors mediate different behaviors of opposite valence. Specifically, D1 receptors mediate the expression of reward-related behaviors while D2 that of aversion-related behaviors (Verharen et al., 2019). Recent studies have also characterized the morphological distinctiveness of MSNs expressing both D1/D2 receptors simultaneously. Here, we did not distinguish between MSN subtypes, and intrinsic morphological differences might have influenced our results. Thus, future

studies need to consider morphological differences between MSNs subtypes and distinguish them during the analysis.

Here, we examined dendritic spine properties at *Zeitgeber19* (time giver), or 21:00h. However, dendritic spines follow daily rhythmic oscillations in their morphology. For example, the extent of branching of synaptic dendrites and their spines changes throughout the day in vertebrates (Frank, 2016). Because of this temporal property, future studies will examine morphological parameters at different time intervals and examine any potential temporal differences.

Per2 and *Per1* have both been linked in having a role in dendritic morphology in Drosophila (Weber et al., 2009). Electron microscopy (EM) studies in Drosophila have also shown that the density and size of synapses are governed by peripheral clocks. Namely, photoreceptor synapses on interneurons are more abundant and larger during the day than the night (Barth et al., 2007). These circadian-dependent morphological changes are also found in motor neurons where the size of synaptic boutons change rhythmically throughout the day. Interestingly, mutations in the *Per* and *Timeless* (*tim*) genes results in a loss of this rhythmic property (Mehnert et al., 2010). Here, we only examined morphological properties in *Bmal1* KO animals and specifically in MSNs. Evidence suggests that multiple circadian genes play a role in neuroplastic properties of other CNS structures, such as hippocampal synapses in rodents. Specifically, synaptic plasticity, or changes in the strength, number, size, or morphological structures (spines and synaptic boutons) of hippocampal synapses are under the control of several circadian genes (Frank, 2016). Thus, future studies will include the examination of other structures in our *Per2* model.

Finally, we examined the morphological properties of striatal dendritic spines in male C57BL/6 mice. However, the striatum is sexually dimorphic particularly in its dopaminergic system and cortico-striatal-thalamic pathway (Andersen et al. 2000, Hietala et al., 1998). Dendritic morphology in the medial prefrontal cortex following chronic stress is also sexually dimorphic and is dependent on estrogen levels (Garrett & Wellman, 2009). Thus, evidence suggests that both the striatum and dendritic properties are morphologically distinct between males and females. Given limitations of measuring the estrus cycle in females due to the COVID-19 pandemic, females were not included in the study. Future studies will incorporate females to examine any potential sexually dimorphic morphological properties.

In summary, we demonstrate that *Bmal1* plays an integral role in motor coordination and striatal dendritic spine morphology. Deletion of *Bmal1* results in aberrated striatal connectivity without affecting the length of dendritic spines. While these results are novel and interesting, the extended and precise role of circadian clock genes in a cell-type, sex, and region-specific MSNs, and their impact on dendritic morphology remains to be further investigated.

References

Albrecht, U. (2012). Timing to perfection: the biology of central and peripheral circadian clocks. Neuron, 74(2), 246–260. doi.org/10.1016/j.neuron.2012.04.006

Alonso Mayor, M. (2021). Behavioral Consequences of Disrupted Circadian Clock Function within the Mouse Striatum (Doctoral dissertation, Concordia University).

Andersen, S., & Teicher, M. (2000). Sex differences in dopamine receptors and their relevance to ADHD, Neuroscience & Biobehavioral Reviews, 24(1), 137–141, https://doi.org/10.1016/S0149-7634(99)00044-5\

Barclay, J. L., Tsang, A. H. & Oster, H. (2012). Interaction of central and peripheral clocks in physiological regulation. Prog Brain Res, 199, 163–181. doi:10.1016/B978-0-444-59427-3.0030-07

Barth, M., Schultze, M., Schuster, C. M., & Strauss, R. (2010). Circadian plasticity in photoreceptor cells controls visual coding efficiency in Drosophila melanogaster. PLoS One, 5(2), e9217.

Berson, D. M., Dunn, F. A., & Takao, M. (2002). Phototransduction by retinal ganglion cells that set the circadian clock. Science, 295(5557), 1070-1073.

Chauhan, R., Chen, K. F., Kent, B. A., & Crowther, D. C. (2017). Central and peripheral circadian clocks and their role in Alzheimer's disease. Disease Models & Mechanisms, 10(10), 1187-1199.

Clemenzi, M. N., Martchenko, A., Loganathan, N., Erika, K. T., Brubaker, P. L., & Belsham, D. D. (2020). Analysis of Western diet, palmitate and *BMAL1* regulation of neuropeptide Y expression in the murine hypothalamus and *BMAL1* knockout cell models. Molecular and Cellular Endocrinology, 507, 110773.

Cronin, P., McCarthy, M. J., Lim, A. S., Salmon, D. P., Galasko, D., Masliah, E., ... & Desplats, P. (2017). Circadian alterations during early stages of Alzheimer's disease are associated with aberrant cycles of DNA methylation in *BMAL1*. Alzheimer's & Dementia, 13(6), 689-700.

de Zavalia, N., Schoettner, K., Goldsmith, J. A., Solis, P., Ferraro, S., Parent, G., & Amir, S. (2021). *Bmal1* in the striatum influences alcohol intake in a sexually dimorphic manner. Communications biology, 4(1), 1-13.

Dibner, C., Schibler, U., & Albrecht, U. (2010). The Mammalian Circadian Timing System: Organization and Coordination of Central and Peripheral Clocks. Annual Review of Physiology, 72, 517–549. https://doi.org/10.1146/annurev-physiol-021909-135821

Frank, M. G. (2016). Circadian regulation of synaptic plasticity. Biology, 5(3), 31.

Frederick, A., Goldsmith, J., de Zavalia, N., & Amir, S. (2017). Mapping the co-localization of the circadian proteins PER2 and *BMAL1* with enkephalin and substance P throughout the rodent forebrain. PLoS One, 12(4), e0176279.

Garey, L. J., Ong, W. Y., Patel, T. S., Kanani, M., Davis, A., Mortimer, A. M., ... & Hirsch, S. R. (1998). Reduced dendritic spine density on cerebral cortical pyramidal neurons in schizophrenia. Journal of Neurology, Neurosurgery & Psychiatry, 65(4), 446-453.

Garmabi, B., Vousooghi, N., Vosough, M., Yoonessi, A., Bakhtazad, A., & Zarrindast, M. R. (2016). Effect of circadian rhythm disturbance on morphine preference and addiction in male rats: involvement of period genes and dopamine D1 receptor. Neuroscience, 322, 104-114.

Garrett, J. E., & Wellman, C. (2009). Chronic stress effects on dendritic morphology in medial prefrontal cortex: sex differences and estrogen dependence. Neuroscience, 162(1), 195-207.

Hamida, S. B., Mendonça-Netto, S., Arefin, T. M., Nasseef, M. T., Boulos, L. J., McNicholas, M., ... & Kieffer, B. L. (2018). Increased alcohol seeking in mice lacking *Gpr88* involves dysfunctional mesocorticolimbic networks. Biological psychiatry, 84(3), 202-212.

Hastings, M. H., Maywood, E. S., & Brancaccio, M. (2019). The Mammalian Circadian Timing System and the Suprachiasmatic Nucleus as Its Pacemaker. Biology, 8(1), 13. https://doi.org/10.3390/biology8010013

Hietela. J., Pohjalainen, T., Juha, O., Kjell, N., Erkka, S. (1998). Sex Differences in the Striatal Dopamine D2 Receptor Binding Characteristics in Vivo. American Journal of Psychiatry, 155(6), 768–773.

Hood, S., & Amir, S. (2017). Neurodegeneration and the circadian clock. Frontiers in aging neuroscience, 9, 170.

Hood, S., Cassidy, P., Cossette, M. P., Weigl, Y., Verwey, M., Robinson, B., ... & Amir, S. (2010). Endogenous dopamine regulates the rhythm of expression of the clock protein PER2 in the rat dorsal striatum via daily activation of D2 dopamine receptors. Journal of neuroscience, 30(42), 14046-14058.

Ikeda, M., Hojo, Y., Komatsuzaki, Y., Okamoto, M., Kato, A., Takeda, T., & Kawato, S. (2015). Hippocampal spine changes across the sleep–wake cycle: corticosterone and kinases. Journal of Endocrinology, 226(2), M13-M27.

Jasinska, M., Grzegorczyk, A., Jasek, E., Litwin, J. A., Kossut, M., BarbackaSurowiak, G., et al. (2014). Daily rhythm of synapse turnover in mouse somatosensory cortex. Acta Neurobiol. Exp. (Wars) 74, 104–110.

Jasinska, M., Grzegorczyk, A., Woznicka, O., Jasek, E., Kossut, M., BarbackaSurowiak, G., et al. (2015). Circadian rhythmicity of synapses in mouse somatosensory cortex. Eur. J. Neurosci. 42, 2585–2594. doi: 10.1111/ejn.13045

Johnson CH, Golden SS, Ishiura M, Kondo T. Circadian clocks in prokaryotes. Mol Microbiol. 1996 Jul;21(1):5-11. doi: 10.1046/j.1365-2958.1996.00613.x. PMID: 8843429.

Kim, M., De La Pena, J. B., Cheong, J. H., & Kim, H. J. (2018). Neurobiological functions of the period circadian clock 2 gene, Per2. Biomolecules & Therapeutics, 26(4), 358.

Kline, R. B. (2009). Becoming a behavioural science researcher: A guide to producing research that matters. New York, NY: Guilford Press.

Krzeptowski, W., Hess, G., & Pyza, E. (2018). Circadian plasticity in the brain of insects and rodents. Frontiers in Neural Circuits, 12, 32.

Lavebratt, C., Sjöholm, L. K., Partonen, T., Schalling, M., & Forsell, Y. (2010). PER2 variation is associated with depression vulnerability. American Journal of Medical Genetics Part B: Neuropsychiatric Genetics, 153(2), 570-581.

Maroteaux, G., Arefin, T. M., Harsan, L. A., Darcq, E., Ben Hamida, S., & Kieffer, B. L. (2018). Lack of anticipatory behavior in *Gpr88* knockout mice showed by automatized home cage phenotyping. Genes, Brain and Behavior, 17(8), e12473.

Mehnert, K. I., Beramendi, A., Elghazali, F., Negro, P., Kyriacou, C. P., & Cantera, R. (2007). Circadian changes in Drosophila motor terminals. Developmental Neurobiology, 67(4), 415-421.

Meirsman, A. C., Ben Hamida, S., Clarke, E., de Kerchove d'Exaerde, A., Darcq, E., and Kieffer, B. L. (2019). *GPR88* in D1R-Type and D2R-Type Medium Spiny Neurons Differentially Regulates Affective and Motor Behavior. eNeuro 6, ENEURO.0035-19.2019. doi: 10.1523/ENEURO.0035-19.2019.

Meirsman, A. C., Le Merrer, J., Pellissier, L. P., Diaz, J., Clesse, D., Kieffer, B. L., et al. (2016a). Mice Lacking *GPR88* Show Motor Deficit, Improved Spatial Learning, and Low Anxiety Reversed by Delta Opioid Antagonist. Biological

Moriya, S., Tahara, Y., Sasaki, H., Hamaguchi, Y., Kuriki, D., Ishikawa, R., ... & Shibata, S. (2014). Effect of quetiapine on Per1, Per2, and *Bmal1* clock gene expression in the mouse amygdala and hippocampus. Journal of pharmacological sciences, 14071SC.

Perez-Cruz, C., Simon, M., Flügge, G., Fuchs, E., & Czéh, B. (2009). Diurnal rhythm and stress regulate dendritic architecture and spine density of pyramidal neurons in the rat infralimbic cortex. Behavioural brain research, 205(2), 406-413.

Quintana, A., Sanz, E., Wang, W., Storey, G. P., Güler, A. D., Wanat, M. J., et al. (2012). Lack of *GPR88* enhances medium spiny neuron activity and alters motor- and cue-dependent behaviors. Nature Neuroscience 15, 1547–1555. doi: 10.1038/nn.3239

Reppert, S. M. & Weaver, D. R. (2001). Molecular analysis of mammalian circadian rhythms. Annu Rev Physiol, 63, 647–676. doi:10.1146/annurev.physiol.63.1.647

Risher, W. C., Ustunkaya, T., Singh Alvarado, J., & Eroglu, C. (2014). Rapid Golgi analysis method for efficient and unbiased classification of dendritic spines. PloS one, 9(9), e107591.

Rusak, B., & Zucker, I. (1979). Neural regulation of circadian rhythms. Physiological reviews, 59(3), 449-526.

Schoettner, K., Alonso, M., Button, M., Goldfarb, C., Herrera, J., Quteishat, N., ... & Amir, S. (2022). Characterization of Affective Behaviors and Motor Functions in Mice With a Striatal-Specific Deletion of Bmal1 and Per2. Frontiers in physiology, 1157.

Simola, N., Morelli, M. & Carta, A. R. (2007). The 6-hydroxydopamine model of Parkinson's disease. Neurotox Res, 11(3), 151–167. doi:10.1007/BF03033565

Smith, D. L., Pozueta, J., Gong, B., Arancio, O., & Shelanski, M. (2009). Reversal of long-term dendritic spine alterations in Alzheimer disease models. Proceedings of the National Academy of Sciences, 106(39), 16877-16882.

Takahashi, J. S. (2017). Transcriptional architecture of the mammalian circadian clock. Nature Reviews Genetics, 18, 164–179.

Tonelli, D., Mayo, O., Boender, A., Armirotti, A., (2019), Deletion of astrocytic *BMAL1* results in metabolic imbalance and shorter lifespan in mice, WILEY, 68(6), 1131–1147. https://doi.org/10.1002/glia.23764

Valdés-Tovar, M., Estrada-Reyes, R., Solís-Chagoyán, H., Argueta, J., Dorantes-Barrón, A. M., Quero-Chávez, D., ... & Benítez-King, G. (2018). Circadian modulation of neuroplasticity by melatonin: a target in the treatment of depression. British journal of pharmacology, 175(16), 3200-3208.

Verharen, J. P., Adan, R. A., & Vanderschuren, L. J. (2019). Differential contributions of striatal dopamine D1 and D2 receptors to component processes of value-based decision making. Neuropsychopharmacology, 44(13), 2195-2204.

Vitaterna, M. H., Takahashi, J. S., & Turek, F. W. (2001). Overview of circadian rhythms. Alcohol Research & Health, 25(2), 85.

Weber, P., Kula-Eversole, E., & Pyza, E. (2009). Circadian control of dendrite morphology in the visual system of Drosophila melanogaster. PLoS One, 4(1), e4290.

Zaqout, S., & Kaindl, A. M. (2016). Golgi-Cox staining step by step. Frontiers in neuroanatomy, 10, 38.

Zaja-Milatovic, S.; Milatovic, D.; Schantz, A. M.; Zhang, J.; Montine, K. S.; Samii, A.; Deutch, A. Y.; Montine, T. J. (2005). Dendritic degeneration in neostriatal medium spiny neurons in Parkinson disease. Neurology, 64(3), 545–547. doi:10.1212/01.WNL.0000150591.33787.A4

Appendix A: Rotarod descriptive statistics and analyses of variance source tables

Table A1

Descriptives and confidence intervals for total time spent on Rotarod

					95% Confidence Interval for Mean	
	N	Mean	Std. Deviation	Std. Error	Lower Bound	Upper Bound
WT	3	601	150.369	86.815	227.461	974.538
HET	4	679	36.724	18.362	620.563	737.436
KO	4	449	122.732	61.366	253.704	644.295
Total	11	574	142.563	42.984	478.315	669.866

Table A2

Repeated Measure Analysis of Variance Results of Total Time Spent on Rotarod

Source		Type III Sum of Squares	df	Mean Square	F	Sig.	Partial Eta Squared	Noncent. Parameter	Observed Power[a]
RPM	Sphericity Assumed	3455.592	3	1151.8	11.81	<.001	.596	35.436	.998
	Greenhouse-Geisser	3455.592	2.038	695.3	11.81	<.001	.596	24.077	.984
RPM * Genotype	Sphericity Assumed	419.252	6	69.875	.717	.640	.152	4.299	.229
	Greenhouse-Geisser	419.252	4.077	102.84	.717	.595	.152	2.921	.185
Error(RPM)	Sphericity Assumed	2340.364	24	97.515					
	Greenhouse-Geisser	2340.364	16.30	143.52					

Note. Computed using alpha = .05

Appendix B: Dendritic parameters descriptive statistics and analyses of variance source tables

Table B1

Tests of Homogeneity of Variance for Dendritic Parameters

		Levene's Statistic	df1	df2	Sig.
Average Density	Based on Mean	.040	2	114	.961
Junctions	Based on Mean	2.711	2	114	.071
Average Length	Based on Mean	.537	2	113	.586
Average Minimum Length	Based on Mean	.329	2	110	.720
Average Maximum Length	Based on Mean	.192	2	114	.825

Table B2

Analysis of Variance with Multiple Comparisons using Tukey HSD

Dependent Variable	(I) Genotype	(J) Genotype	Mean Difference (I-J)	Std. Error	Sig.	95% Confidence Interval	
						Lower Bound	Upper Bound
Average Density	WT	HET	.046	.022	.094	-.006	.099
		KO	.107*	.022	<.001	.054	.160
	HET	WT	-.046	.022	.094	-.099	.006
		KO	.060*	.022	.022	.007	.114
	KO	WT	-.107*	.022	<.001	-.160	-.054
		HET	-.060*	.022	.022	-.114	-.007
Number of Junctions	WT	HET	1.765	1.255	.341	-1.22	4.75
		KO	5.334*	1.263	<.001	2.33	8.33
	HET	WT	-1.765	1.255	.341	-4.75	1.22
		KO	3.569*	1.271	.016	.55	6.59
	KO	WT	-5.334*	1.263	<.001	-8.33	-2.33
		HET	-3.569*	1.271	.016	-6.59	-.55
Average Length	WT	HET	-.068	.049	.355	-.187	.049
		KO	.047	.049	.614	-.071	.165
	HET	WT	.068	.049	.355	-.049	.187
		KO	.116	.050	.061	-.004	.236
	KO	WT	-.047	.049	.614	-.165	.071
		HET	-.116	.050	.061	-.236	.004
Average Minimum Length	WT	HET	.033	.026	.413	-.029	.097
		KO	.005	.026	.975	-.057	.069
	HET	WT	-.033	.026	.413	-.097	.029
		KO	-.028	.026	.550	-.092	.035
	KO	WT	-.005	.026	.975	-.069	.057
		HET	.028	.026	.550	-.035	.092
Average Maximum Length	WT	HET	-.388	.164	.052	-.780	.002
		KO	-.065	.165	.918	-.459	.328
	HET	WT	.388	.164	.052	-.002	.780
		KO	.323	.167	.133	-.073	.720
	KO	WT	.065	.165	.918	-.328	.459
		HET	-.323	.167	.133	-.720	.073

Note. The mean difference is significant at the 0.05 level.

Appendix C: Dendritic parameters source tables for *Gpr88*+/+ and *Gpr88* Cre animals

Table C1

Tests of Homogeneity of Variance for Dendritic Parameters

		Levene's Statistic	df1	df2	Sig.
Average Density	Based on Mean	2.129	1	66	.149
Junctions	Based on Mean	.150	1	64	.700
Average Length	Based on Mean	.638	1	64	.427
Average Minimum Length	Based on Mean	.098	1	62	.756
Average Maximum Length	Based on Mean	.595	1	66	.443

Table C2

ANOVA Source Table for Gpr88 +/+ and Gpr88 Cre Animals

		Sum of Squares	df	Mean Square	F	Sig.
Average Density	Between Groups	.001	1	.001	.085	.771
	Within Groups	.733	66	.011		
	Total	.734	67			
Number of Junctions	Between Groups	.112	1	.112	.002	.962
	Within Groups	3129.418	64	48.897		
	Total	3129.530	65			
Average Length	Between Groups	.082	1	.082	1.466	.230
	Within Groups	3.598	64	.056		
	Total	3.681	65			
Average Minimum Length	Between Groups	.006	1	.006	.430	.514
	Within Groups	.856	62	.014		
	Total	.862	63			
Average Maximum Length	Between Groups	.711	1	.711	.733	.395
	Within Groups	64.035	66	.970		
	Total	64.746	67			

Note. Gpr88 +/+ (*n* = 4) & *Gpr88* Cre (*n* = 3)